Sensors and Materials, Vol. 25, No. 7 (2013) 509–518
MYU Tokyo

S & M 0944

A High-Density Beam-Forming Acoustic Sensor Array Design Based on Acoustoelectric Effect

Renhuan Yang, Aiguo Song* and Baoguo Xu

School of Instrument Science and Engineering, Southeast University, 317 Zhongxin Buiding, No. 2 Si Pai Lou, Nanjing, Jiangsu Province 210096, China

(Received November 1, 2012; accepted February 7, 2013)

Key words: sensor array, beam forming, acoustoelectric effect, nondestructive testing, acoustic detection

It is important to nondestructively detect the operating electrical equipment of a power grid. Acoustic detection is one of the most effective methods of electric equipment malfunction detection. A single sensor can only detect acoustic serials. A sensor array is needed for imaging acoustic field and acoustic source localization. Traditional acoustic measuring devices are available depending on the application. These devices, however, are limited by their specific physical properties, often leading to limited bandwidth, susceptibility to damage under high pressure and fragility to fabrication. Thus, it is difficult to integrate a high-intensity, large-scale acoustic sensor array. In this paper, a sensor array based on acoustoelectric effect is proposed for noninvasively imaging acoustic fields. This device can use material with excellent fabrication properties as an acoustic sensitivity element, so photolithography can be adopted to integrate a high-intensity, large-scale acoustic sensor array. A focused spherical sensor array with a large focal length and a small focal spot is designed for imaging acoustic fields. The beam pattern calculation method is provided. Computer simulation results indicate that a beam with a large focal length of 180 cm and a small ellipse focal spot of 4.52 cm^2 can be formed using the proposed sensor array. Computer simulation of imaging a target acoustic field shows that a clear map of the target acoustic field can be obtained by noninvasively scanning the acoustic field with the proposed sensor array.

1. Introduction

An uninterruptible power supply is one important requirement for the electric power grid. One main electrical equipment, i.e., a transformer that stops working suddenly because of malfunction may bring millions of Renminbi (RMB) loss to a power supply company and have a great impact on society.[1,2] Thus, the noninvasive test of operating electrical equipment in a power grid is of importance. Acoustic detection is one of the most effective noninvasive detection methods for electric equipment malfunction.[2–5]

*Corresponding author: e-mail: a.g.song@seu.edu.cn

Many electrical equipment malfunctions, such as poor contact, screw loosing, and partial discharge, will generate abnormal sound.[2,3] Although conventional acoustic measuring devices, such as membrane, needle, and fiber optic hydrophones, have been successfully employed in a variety of noninvasive testing applications, each has drawbacks. They exhibit low sensitivity, reduced bandwidth, high damage susceptibility, and fragility to fabrication.[6–8] Thus, it is difficult to integrate a high-intensity, large-scale acoustic sensor array. Besides, previous hydrophones that relied on exclusively piezoelectric materials embedded between two semiconductors to measure acoustic wave had poor sensitivity and could only detect the acoustic power without phase information.[9–12] Recently, a prototype acoustic sensor based on an acoustoelectric (AE) effect has generated considerable interest.[13] Initial experiment indicates that this kind of device has attractive attributes not typically seen with other hydrophones: simple construction, low cost, decent sensitivity, and resistance to damage at high-intensity acoustic fields.[13–15] However, a single sensor can only detect one-dimensional acoustic serials. For noninvasively imaging acoustic field and acoustic source localization, a sensor array is desired.

In this paper, we propose a sensor array based on AE effect for noninvasively imaging acoustic fields. This device can use material with excellent fabrication properties, i.e., indium tin oxide (ITO), as sensitivity acoustic elements, so photolithography can be adopted to integrate a high-intensity, large-scale sensor array. A focused spherical sensor array with a large focal length and a small focal spot is designed for imaging acoustic fields noninvasively. This kind of large-scale acoustic sensor array has important potential applications in noninvasive test of operating electrical equipment.

2. Materials and Methods

2.1 *Principle of acoustic sensor based on AE effect*

The principle of the acoustic sensor based on the AE effect is illustrated in Fig. 1. An alternating bias current (~100 Hz) was applied across the sensitivity material (ITO) between two gold electrodes to generate a current density distribution $\boldsymbol{J}^{\mathrm{I}}(x, y, z)$. The acoustic wave propagating in the sensitivity material with charged particles inside induce a change $\Delta\rho(x, y, z, t)$ in the electric resistivity of the sensitivity material due to the AE effect.[16–19]

$$\Delta\rho(x, y, z, t) = -K\rho_0(x, y, z, t)P(x, y, z, t) \tag{1}$$

Here, K is interaction constant, ρ_0 is inherent electric resistivity of the sensitivity material, and $P(x, y, z, t)$ is the acoustic pressure.[17–19] The voltage perturbation due to the resistivity change in the sensitivity material was measured using the same electrode pair injecting the bias current. According to the lead field theory, the measured voltage of lead with lead field $\boldsymbol{J}^{\mathrm{L}} = \boldsymbol{J}^{\mathrm{I}}(x, y, z)$ due to a current density distribution $\boldsymbol{J}^{\mathrm{I}}(x, y, z)$ can be written as[20,21]

$$V = \iiint_V \rho\boldsymbol{J}^{\mathrm{L}}(x, y, z) \bullet \boldsymbol{J}^{\mathrm{I}}(x, y, z)\mathrm{d}x\mathrm{d}y\mathrm{d}z. \tag{2}$$

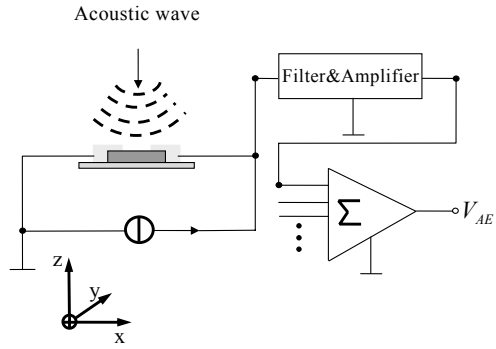

Fig. 1. Schematic of the acoustic sensor based on AE effect.

The voltage was measured using the same electrode pair injecting the bias current so $\boldsymbol{J}^{\mathrm{L}} = \boldsymbol{J}^{\mathrm{I}}$. Since the region of the sensitivity material is very small, we can assume ρ, $\boldsymbol{J}^{\mathrm{I}}$, and P as constant in the sensitivity region. By combining eqs. (1) and (2), we can obtain eq. (3) on the voltage measurement with existing AE effect:

$$V = \iiint_V \rho_0(1 - KP)|\boldsymbol{J}(x,y,z)|^2 \mathrm{d}x\mathrm{d}y\mathrm{d}z \approx \rho_0(1 - KP(t))|\boldsymbol{J}|^2 V_S$$
$$= \rho_0|\boldsymbol{J}|^2 V_{\mathrm{S}} - \rho_0 KP(t)|\boldsymbol{J}|^2 V_{\mathrm{S}} \tag{3}$$

where V_{S} is the volume of the sensitivity region. In eq. (3), the first term, which is generated by inherent electric resistivity, is called the baseline signal. The other term, which is generated by the electrical resistivity change due to the AE effect, is called the AE signal. The baseline signal is a low-frequency signal corresponding to the injected current, whereas the AE signal is a high-frequency signal corresponding to detected acoustic wave. Thus, they can be easily separated by a high-pass or band-pass filter.[22–24] The AE signal equation is written as

$$V_{\mathrm{AE}} = \rho_0 K|\boldsymbol{J}|^2 V_{\mathrm{S}} P(t). \tag{4}$$

Equation (4) gives the linear relationship between the detected acoustic signal and the measured AE signal. Thus, we can measure the acoustic signal linearly by measuring the AE signal.

2.2 *A focused spherical sensor array design*

The focused spherical sensor array is illustrated by Fig. 2. Sensor elements are integrated in a focused spherical base made of waveguide plexiglass. An acoustic attenuation material is used to reduce the influence of echo after the acoustic wave passes the waveguide. In fact, the echo has been separated from the AE signal by using

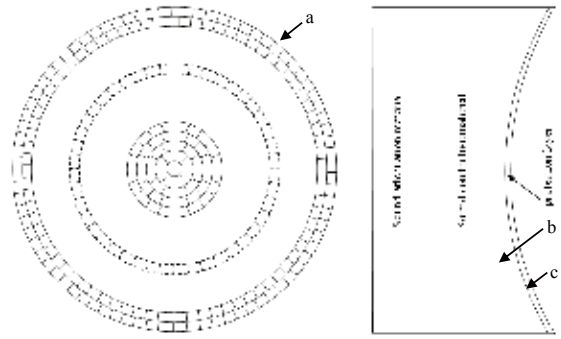

Fig. 2. Illustration of the focused spherical acoustic sensor array (a, sensor elements; b, focused spherical base; c, concave).

the waveguide to generate an interval.[25] Thus, the influence of echo can be neglected. In the present study, the radius of the focused spherical base is set as 1 m; the radius of curvature (concave radius) is 2 m. The sockets for embedding sensor elements are made on the concave perpendicular to the concave radius. After all the sensor elements are embedded in the spherical base, the completed array is spin-coated with Cytop® for waterproofing and insulation[15], i.e., for protection layer as shown in Fig. 2.

The design of the sensor element is illustrated by Fig. 3. a) The plexiglass base/film is coated with photoresist (PR). b) The base is then coated with indium ITO with a thickness of 100 nm. c) The sensitivity region is formed by marking the ITO with PR. The sensitivity patterns of sensor elements are created in the ITO by means of a positive photolithographic process. d) The unmarked ITO is etched away with hydrochloric acid and nitric acid mixed in water (H_2O:HCl:HNO_3 = 5:5:1). e) The PR is then washed away with acetone, exposing the pattern in ITO on the base. f) The two ends of the ITO pattern are overlaid with gold electrodes, leaving the middle part of the pattern unaltered as the sensitivity zone. Finally, the lead wires are soldered to the gold electrodes. After that, the whole integrated sensor array is spin-coated with Cytop® for waterproofing and insulation.[13–15] The dimension of the sensor element is 4×4 mm^2, and the sensitivity zone, 1×1 mm^2. All the sensor element outputs were first filtered to extract the AE signals, and then all the AE signals were amplified and summed up together using an additional circuit.[26]

2.3 *Beam pattern calculation method of the focused spherical sensor array*

The solution of acoustic beam pattern of a focused transducer was reported and discussed by Lucas and Muir, and Chen *et al*.[27,28] Because the sensitivity element is very small and integrated with high density, the sensitivity element can be assumed to be infinitely small. Applying the mean field theory, the accumulation of a large number of small elements can be approximately calculated from the corresponding integration,[29,30] so the beam pattern of the focused spherical sensor array in a polar coordination system

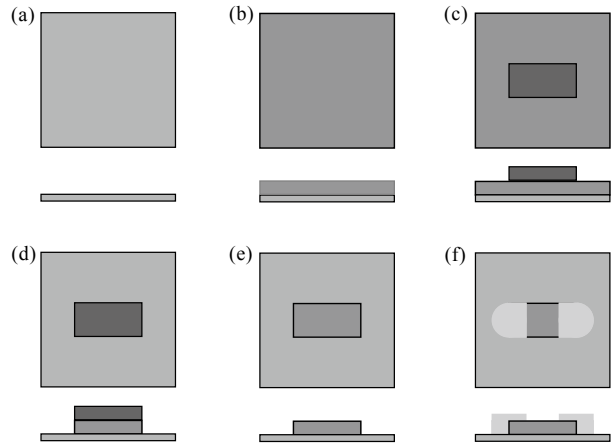

Fig. 3. Sensor element design of the beam-forming acoustic sensor array.

can be estimated as[25–28]

$$b(r,\theta) = ip_0(ka^2/r)\exp(-ikr)\int_{u=0}^{1}\exp(-i\frac{ka^2}{2r}(1-\frac{r}{R_0}\cos(\theta))u^2)uJ_0(ka\sin(\theta u))\mathrm{d}u \quad (5)$$

where k is the wave number, a is the radius of the sensor array, R_0 is the concave radius, and J_0 is the first-order Bessel function.[27,28] The −6 dB beam diameter can be estimated as $B_D = 1.02Fc/(fD)$, where F is the focus length, c is the sound velocity in the media, f represents central frequency, and D is the diameter of the sensor array.

2.4 *Computer simulation*

For the calculation of beam pattern, a numerically convergent solution to eq. (5) with error smaller than 0.01 was provided by Chen *et al.*[28] We applied Chen *et al.*'s method to calculate the beam pattern of the focused spherical sensor array in the present simulation study. An acoustic field imaging can be obtained by performing a three-dimensional raster scan with the sensor array. The simulation of imaging a controllable target acoustic field using the proposed focused spherical sensor array was conducted to investigate the feasibility of imaging the acoustic field by using this kind of sensor array. The acoustic field generated by two parallel focused transducers of 4 cm diameter, 20 cm focus length, and 10 kHz frequency was simulated as the target acoustic field using the same method.[28] The acoustic field imaging was simulated by convolving the target acoustic field with the beam pattern of the sensor array.[25] The convolution calculation can be accelerated by applying the fast Fourier transformation (FFT) method. The origin of the coordinate system was set at the center of the concave.

3. Results

3.1 *Beam pattern of the focused spherical sensor array*

The beam pattern of the focused spherical sensor array is shown in Fig. 4. We can see that an acoustic beam pattern with a small focus spot at 180 cm from the center of the sensor array along the beam axis can be obtained by using the focused spherical sensor array. The full widths at half maximum (FWHMs) of the acoustic focus spot are 6.36 cm in the beam axis and 0.71 cm in the lateral axis. It is noteworthy that the lateral direction's spatial resolution is better than the beam axis', so we can utilize lateral scan to improve the spatial resolution for acoustic field imaging.

3.2 *Simulation results for imaging a target acoustic field*

The simulated acoustic field is displayed in Fig. 5(a). The acoustic field imaging is shown in Fig. 5(b). By comparing the acoustic field imaging and the target acoustic

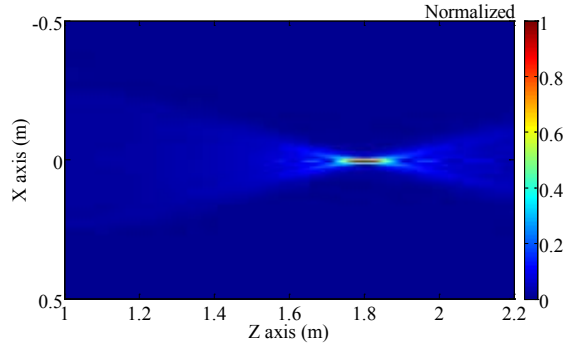

Fig. 4. Beam pattern simulation result of the focused spherical sensor array. *Z* axis corresponds to the beam axis and *X* axis is the lateral axis.

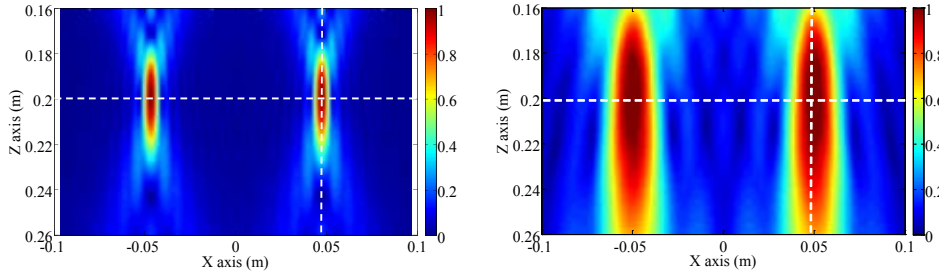

(a) (b)

Fig. 5. Controllable target acoustic field (a) and (b) imaging result by raster scanning the target acoustic field in *X*-*Z* plane using the proposed sensor array.

field, it is clear that the imaging can well represent the target acoustic field. A clear imaging of the target acoustic field can be obtained by using the proposed sensor array. We also note that the focus spots of the target acoustic field are enlarged due to the point spread function of the sensor array.[25]

For direct comparisons, Figs. 6 and 7 show line profiles of the target acoustic field and the imaging along the beam axis and the lateral direction, respectively. From Fig. 6, we can see that the imaging profiles in the beam axis can follow the target acoustic field and the focus spot at $Z = 0.2$ m can be clearly discerned, but the focus spot imaging is lengthened owing to the smoothing effect of the long (6.36 cm) focus spot of the sensor array. As shown in Fig. 7, the imaging profiles in the lateral direction can well represent the target acoustic field. The focus and side lobes can be clearly discerned from the lateral profiles. Because the dimension of the focus spot is far larger than that in the lateral direction, the smoothing effect of the long elliptic focus spot can be improved by utilizing lateral scan.[13]

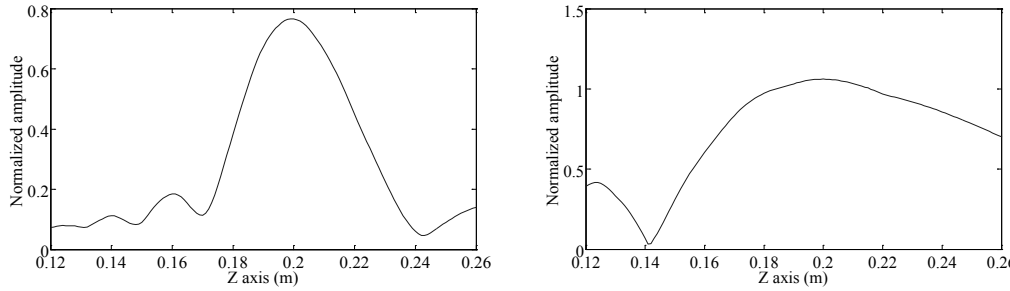

Fig. 6. Beam direction profiles (as marked by the white dotted line in Fig. 5) of target acoustic field (a) and (b) imaging result by using the proposed sensor array.

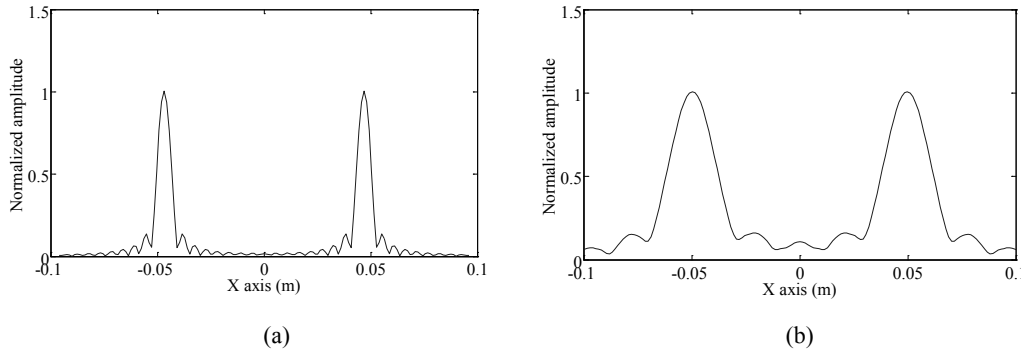

Fig. 7. Lateral profiles (as marked by the white dotted line in Fig. 5) of target acoustic field (a) and (b) imaging result by using the proposed sensor array.

4. Discussion

Noninvasively testing for operating electrical equipment is very important for enhancing electric power supply quality.[1,2] Acoustic detection as one of the most effective noninvasive testing methods has been widely employed in various applications. Acoustic field imaging and source localization play key roles in electrical equipment state assessment and malfunction diagnosis.[2–5] However, it is very difficult to image an acoustic field by using a single sensor. Thus, a beam-forming sensor array is proposed for noninvasive acoustic field imaging and source localization. Recently, a prototype acoustic sensor based on the AE effect has attracted considerable interest.[12–15] Initial experiments have indicated that this kind of acoustic sensor based on the AE effect has attractive attributes: simple construction, low cost, high sensitivity, and resistance to damage at high-intensity acoustic fields.[13–15] Optimization of the acoustoelectric sensor for mapping an ultrasound beam with consideration of hydrophone shape, material relative resistivity, thickness, and lateral width has been reported.[14] The sensitivity and signal-to-noise ratio (SNR) can be improved by optimizing these parameters. This type of AE sensor fabrication method using photolithography has also been provided in ref. 15. Different from these reported research studies, our study focuses on designing a beam-forming acoustic sensor array with a large focal length and a small focal spot. This sensor array can use sensitivity material with excellent fabrication properties as acoustic sensitivity elements, so a high-intensity, large-scale sensor array can be integrated by adopting photolithography.[15] In practice, a sinusoidal bias current (~100 Hz) was applied across the sensitivity zone between two gold electrodes because the oscillating field limits the adverse effects associated with the direct current, such as electrode polarization and hydrolysis.[22–24] The sinusoidal current injections are synchronously triggered, and the AE signals generated around the peaks of the sinusoidal current injections are synchronously acquired to obtain good SNR.[22,23] For easily separating the AE signal from the injected sinusoidal current by using a highpass or bandpass filter, the frequency of the bias current should be lower than that of the detected acoustic signal.[22–31] A large-scale addition circuit can be used to summarize the AE signal of all the sensor elements after amplifying and adjusting to form an acoustic focus spot.[26] This beam forming can also be processed by a computer using the collected AE signals of all the sensor elements. Because the focus spot in the beam axis is relatively big in comparison with that in the lateral direction, the spatial resolution in the beam axis is not as good as that in the lateral direction. The focus spot of the sensor array can be improved by increasing the array diameter and decreasing the concave radius.[25] However, it is noteworthy that decreasing the concave radius will shorten the focus length, which will reduce the detection depth of the sensor array.

5. Conclusions

In this paper, a beam-forming sensor array is proposed for noninvasively imaging acoustic fields and acoustic source localization. ITO, which has excellent fabrication properties, can be used to make the sensitivity element, so that photolithography can

be adopted to integrate a high-intensity, large-scale acoustic sensor array. A focused spherical sensor array is designed for noninvasively imaging acoustic fields. The acoustic sensor array has a large-focal length and a small focal spot. Computer simulation results show that a beam with a large focal length of 180 cm and a small ellipse focal spot of 4.52 cm^2 can be obtained using the proposed sensor array. Computer simulation results also show that a clear imaging of the target acoustic field can be obtained by performing a raster scanning with the proposed sensor array. This type of large-focal-length, small-focal-spot acoustic sensor array has important potential application in noninvasive detection and assessment of operating electrical equipment. Further experimental study will be needed to fully test the feasibility and capability of the proposed beam-forming acoustic sensor array.

Acknowledgements

This work was supported in part by the NSF of China (Nos. 61272379, 61104206, 61302131, and 11005047), N. K. T. R&D Program (No. 2008BAI50B00), China High-Tech Plan (No. 2008AA040202), Key Project of M E of China (No. 107053), Key Project of NSF of Jiangsu Province (Nos. BK2010063, BK2010423, and BE2012740), and SRF of SEU. RY was supported in part by the IPGE of Jiangsu Province (No. CX08B 050Z), the SRF of the Graduate School of SEU (No. YBPY1108), and scholarship from CSC ((2009)3012), and RD Project of China Southern Power Grid.

References

1 H. Wei, H. Sasaki, J. Kubokawa and R. Yokoyama: IEEE Trans. Power Syst. **15** (2000) 396.
2 J. Ramirez-Nino and A. Pascacio: 6th International Symposium on Measurement Techniques for Multiphase Flows 2008, (Measurement Science & Technology, 2009) p. 15.
3 M. K. Chen, C. Y. Cheng and W. Y. Chang: 17th Biennial IEEE International Symposium on Electrical Insulation 2008, (IEEE, 2008) p. 361.
4 T. Han, X. J. Ji and W. K. Shi: Sens. Mater. **18** (2006) 173.
5 A. Garg, K. Rajanna: Sens. Mater. **17** (2005) 423.
6 G. Harris: Proceedings of the IEEE UFFC 1999, (IEEE, 2008) p. 1341.
7 A. J. Coleman: Ultrasound Med. Biol. **24** (1998) 143.
8 M. E. Schafer, T. L. Kraynak and P. A. Lewin: Proceedings of the IEEE Ultrasonics Symposium, (IEEE, 1990) p. 1623.
9 D. Dietz, L. Busse and M. Fife: IEEE Trans. Ultrason. Ferroelectr. Freq. Control **35** (1988) 146.
10 L. Busse and J. Miller: J. Acoust. Soc. Am. **70** (1981) 1377.
11 L. Busse and J. Miller: J. Acoust. Soc. Am. **70** (1981) 1370.
12 H. Zhang and L. Wang: Proc. SPIE, eds. A. A. Oraevsky and L. V. Wang (SPIE, Bellingham, WA, 2004) p. 145.
13 R. S. Witte, T. Hall, R. Olafsson, S. Huang and M. O'Donnell: J. Appl. Phys. **104** (2008) 054701.
14 Z. Wang, P. Ingram, C. Greenlee, R. A. Norwood and R. S. Witte: Medical Imaging 2010: Ultrasonic Imaging, Tomography, and Therapy, Proc. SPIE, eds. J. D'hooge and S. A. McAleavey (SPIE, 2010) p. 76290Q.

15 P. Ingram, C. Greenlee, Z. Wang, R. Olafsson, R. Norwood, R. S. Witte: Medical Imaging 2010: Ultrasonic Imaging, Tomography, and Therapy, Proc. SPIE, eds. Jan D'hooge, Stephen A. McAleavey (SPIE, 2010) p. 76290O.
16 F. Fox, K. Herzfeld and G. Rock: Phys. Rev. **70** (1946) 329.
17 J. Jossinet, B. Lavandier and D. Cathignol: Ultrasonics **36** (1998) 607.
18 B. Lavandier, J. Jossinet and D. Cathignol: Med. Biol. Eng. Comput. **38** (2000) 150.
19 B. Lavandier, J. Jossinet and D. Cathignol: Ultrasonics **38** (2000) 929.
20 J. Malmivuo and R. Plonsey: Bioelectromagnetism: Principles and Applications of Bioelectric and Biomagnetic Fields (Oxford Univ. Press, New York, 1995) p. 148.
21 B. He: Modeling and Imaging of Bioelectrical Activity–Principles and Applications, ed. B. He (Kluwer Academic Publishers, New York, 2004) p. 183.
22 R. S. Witte, R. Olafsson, S. W. Huang and M. O'Donnell: Appl. Phys. Lett. **90** (2007) 163902.
23 R . Olafsson, R. S. Witte, S. W. Huang and M. O'Donnell: IEEE Trans. Biomed. Eng. **55** (2008) 1840.
24 R. Olafsson, R. S. Witte, C. X. Jia, S. W. Huang, K. Kim and M. O'Donnell: IEEE Trans. Ultrason. Ferroelectr. Freq. Control **56** (2009) 565.
25 R. S. C. Cobbold: Foundations of Biomedical Ultrasound-Biomedical Engineering Series, ed. R. S. C. Cobbold (Oxford University Press, Oxford, UK, 2006) p. 96.
26 C. Sumi: Acoustical Science and Technology **30** (2009) 310.
27 B. G. Lucas and T. G. Muir: J. Acoust. Soc. Am. **72** (1982) 1289.
28 X. Chen, K. Q. Schwarz and K. J. Parker: J. Acoust. Soc. Am. **94** (1993) 2979.
29 G. Avitabile, M. Forti, S. Manetti and M. Marini: IEEE Trans. Circ. Syst.-I **38** (1991) 202.
30 Y. Fang, T. G. Kincaid: IEEE Trans. Neural Networks **7** (1996) 996.
31 R. Yang, X. Li, J. Liu and B. He: Phys. Med. Biol. **56** (2011) 3825.